Progress In Electromagnetics Research B, Vol. 81, 183–201, 2018

Burr Distribution for X-Band Maritime Surveillance Radar Clutter

Graham V. Weinberg* **and Charlie Tran**

Abstract—Recent research has shown that the Pareto family of distributions provides suitable intensity models for high resolution X-band maritime surveillance radar clutter. In particular, the two parameter Pareto Type II model has been shown to fit the Australian Defence Science and Technology Group's medium to high grazing angle clutter returns very well. The Pareto Type II model is a special case of a Burr distributional model, which is a three parameter power law statistical model. Hence this paper begins by investigating the fitting of the Burr model to real data. Based upon these results a detailed study of the development of non-coherent sliding window detectors is justified, for operation in such clutter. Several different approaches will be applied to construct the decision rules. These include a transformation approach and direct adaptation of such detectors, designed for operation in exponentially distributed clutter, to the Burr clutter setting. In addition to this, the fact that the Burr distribution is invariant with respect to two of its distributional parameters allows specification of detection processes which have the constant false alarm rate property with respect to these model parameters. Performance analysis, in simulated clutter, of the derived detectors is then examined. This includes performance in the presence of interference and false alarm regulation during clutter power transitions. This is complemented by an application of the decision rules to target detection in real high resolution X-band maritime surveillance radar clutter.

1. INTRODUCTION

In order to design radar detection processes it is necessary to validate statistical models for the resultant environmental radar backscattering. In the context of X-band high resolution maritime surveillance radar, the backscattering in the absence of a target is referred to as clutter. Such clutter is often described as spiky, and there has been much interest in the determination of appropriate statistical models for such clutter. The issue faced by radar engineers and scientists is the selection of a model, which fits into the currently accepted radar clutter model phenomenology and which also allows the constant false alarm rate (CFAR) property to be achieved in homogeneous clutter settings [1]. In the case of non-coherent detection this has proven to be a challenging endeavour. However, with the introduction of the Pareto class of clutter models, it has been possible to address these issues [2].

Validation of the Pareto model for X-band maritime surveillance radar clutter first appeared in [3], and a second independent validation was provided in [4]. These were both in the case of a low grazing angle, with a stationary radar. A third validation was provided by [5], which was for the case of an airborne maritime surveillance radar, operating with a medium to high grazing angle.

This paper reexamines the fit of distributions to maritime surveillance radar clutter. In particular, since the Pareto Type II distributional model is a special case of a Burr distribution, its fit to real sea clutter returns is investigated. The Burr distribution is a three parameter power law type model introduced in [6]. Such a distribution has two shape parameters and one scale parameter. The Pareto Type II model arises when one of these shape parameters is set to unity. Hence it became of interest

Received 18 June 2018, Accepted 9 August 2018, Scheduled 22 August 2018
* Corresponding author: Graham V. Weinberg (graham.weinberg@dst.defence.gov.au).
The authors are with the Defence Science and Technology Group, Australia.

to investigate whether improved fits could be achieved with the Burr distribution, and whether fitting of the three parameter model reduced to the Pareto Type II, implying that it is a sufficient fit for the data under consideration. It will be shown that the Burr model provides a tighter fit to Defence Science and Technology (DST) Group's real X-band maritime surveillance radar clutter returns, which was acquired through the Ingara radar. Ingara is an experimental fully polarimetric X-band imaging radar [7], and analysis of data acquired by it has been reported in [8–10]. The Pareto fit to this data has been documented in [5]. Based upon DST Group's parameter estimates for the Pareto Type II model it has been possible to apply a Pareto Type I approximation to facilitate the development of non-coherent detectors [11–16]. These non-coherent decision processes are in the spirit of [17] and [18], which assess the presence of a target in a cell under test (CUT) based upon a normalised measurement of the clutter level. Based upon validation of the Burr fit to DST Group's Ingara radar clutter, this paper initiates the development of non-coherent sliding window detection processes, for operation in a Burr-distributed clutter environment. In particular, it is of interest to examine whether the CFAR property can be achieved with respect to any of the Burr distributional parameters. Several approaches will be adopted in the construction of the sliding window detection processes. The transformation approach, introduced in [11] and generalised in [12], will be applied to produce two decision rules. The fact that the Burr distribution is invariant with respect to two of its distributional parameters allows the construction of a partial CFAR process, in the spirit of [19]. The direct adaptation approach, examined in [15], will then be used to also produce two detectors. Performance analysis, in both synthetic and real clutters, will then be considered. Towards these objectives, the paper is organised as follows. Section 2 introduces the Burr distribution and discusses its relationship to the Pareto models, while Section 3 investigates the fit of the Burr distribution to DST Group's real X-band clutter. Section 4 then derives a series of non-coherent decision rules, while Section 5 examines their performance in both synthetic and real clutter returns.

2. BURR AND PARETO DISTRIBUTIONS

The purpose of this section is to introduce the Burr distribution and discuss its relationship to the Pareto Type II model, as well as some of its properties useful in the analysis to follow. A non-negative random variable Z has a Burr distribution if its cumulative distribution function is

$$F_Z(t) = \mathbb{P}(Z \leq t) = 1 - \left(\frac{\beta}{\beta + t^\kappa}\right)^\alpha, \tag{1}$$

where α and κ are non-negative shape parameters; β is a non-negative scale parameter; $t \geq 0$. The corresponding probability density function, obtained by differentiating Equation (1), is given by

$$f_Z(t) = \frac{\alpha\beta^\alpha\kappa t^{\kappa-1}}{(\beta + t^\kappa)^{\alpha+1}}. \tag{2}$$

It is clear that by setting κ to unity in Equations (1) and (2) one recovers the Pareto Type II distribution for Z. Thus the Burr model is a three parameter extension of the Pareto Type II distribution, with κ acting as a second shape parameter. In order to understand the impact that κ is having on the underlying Pareto Type II model, it is not difficult to show that if X is a random variable with a Pareto Type II distribution, with cumulative distribution function

$$F_X(t) = 1 - \left(\frac{\beta}{\beta + t}\right)^\alpha, \tag{3}$$

then $Z = X^{\frac{1}{\kappa}}$. Hence the additional shape parameter κ acts as a reciprocal power on the Pareto Type II model, in order to produce the Burr distribution. It is expected that this extra shape parameter will produce a longer tail in the model and consequently tighter fits to real data.

Recall that a random variable Y with a Pareto Type I distribution has cumulative distribution function

$$F_Y(t) = 1 - \left(\frac{\beta}{t}\right)^\alpha, \tag{4}$$

provided $t \geq \beta$, where $\alpha > 0$ is the shape, and $\beta > 0$ is the scale parameter [20]. This model has a non-negative support starting at β, and it can be shown that $Y \stackrel{d}{=} X + \beta$, showing that the Pareto Type I and II models are linearly associated in distribution. The notation $\mathcal{A} \stackrel{d}{=} \mathcal{B}$ means that the random variables $\mathcal{A}$ and $\mathcal{B}$, with common support, have the same distribution function. Fits of the Pareto Type II model to DST Group's Ingara radar clutter resulted in estimates for $\beta \ll 1$. Based upon this, the approach in [2] was to develop non-coherent radar detectors under a Pareto Type I clutter environment, to allow sliding window detectors to be produced with the CFAR property.

Again, with reference to the Burr distribution, if Z is a random variable with distribution function in Equation (1), then it is not difficult to show that, for any $r > 0$, the mean of Z^r is

$$\mathbb{E}(Z^r) = \alpha\beta^{\frac{r}{\kappa}}\mathcal{B}\left(\alpha - \frac{r}{\kappa}, \frac{r}{\kappa} + 1\right), \tag{5}$$

where $\mathcal{B}(\cdot,\cdot)$ is the well-known beta function. This result is necessary for the specification of the signal to clutter ratio (SCR) used in the numerical analysis.

The inverse distribution function technique can be used to derive an expression which facilitates the simulation of a random variable with a Burr distribution [21]. Noting that the inverse of (1) is

$$F_Z^{-1}(t) = \left(\beta\left[[1-t]^{-\frac{1}{\alpha}} - 1\right]\right)^{\frac{1}{\kappa}} \tag{6}$$

it follows that

$$Z \stackrel{d}{=} F_Z^{-1}(1-R) = \left(\beta\left[R^{-\frac{1}{\alpha}} - 1\right]\right)^{\frac{1}{\kappa}}, \tag{7}$$

where R has a uniform distribution on the unit interval. Thus, for given α, β and κ, one generates a random number in the unit interval and applies this in place of R in the right hand side of Equation (7), to produce a realisation of the corresponding Burr distribution.

The kth order statistic (OS) for a series of Burr distributed random variables is required in the derivation of probabilities of false alarm (Pfa) of detectors to follow, so is now examined here. It has been shown in [22] that the kth OS for a random sample from a Pareto Type I distribution is $Y_{(k)} \stackrel{d}{=} \beta W_k^{-\frac{1}{\alpha}}$, where W_k has a beta distribution with parameters $N-k+1$ and k, respectively, where $1 \leq k \leq N$. The latter random variable has density

$$f_{W_k}(t) = \frac{N!}{(N-k)!(k-1)!}t^{N-k}(1-t)^{k-1}, \tag{8}$$

for $t \in [0,1]$.

Hence it is not difficult to show that if $Z_{(k)}$ is the kth OS from a random sample from a Burr distribution then

$$Z_{(k)} \stackrel{d}{=} \left[\beta\left(W_k^{-\frac{1}{\alpha}} - 1\right)\right]^{\frac{1}{\kappa}}, \tag{9}$$

since the Burr distribution is related to the Pareto Type I through a power transformation, and also due to the linear association between the Pareto Type I and II distributions.

Next the fitting of the Burr distribution to DST Group's Ingara data is examined.

3. BURR DISTRIBUTIONAL FITS TO INGARA DATA

This section now examines the fit of the three parameter Burr model to real data and compares it with that of the Pareto Type II. In addition to this, the fits of two popular models for X-band radar clutter are also examined. The first of these is the well-known K-distribution [23]. A random variable $\mathcal{K}$ is said to have a K-distribution, with nonnegative shape and scale parameters ν and c, if its density is

$$f_{\mathcal{K}}(t) = \frac{2c}{\Gamma(\nu)}\left(\frac{ct}{2}\right)^{\nu} K_{\nu-1}(ct), \tag{10}$$

where Γ is the Gamma function, and K_ν is the modified Bessel function of the second kind of order ν, for $t \geq 0$. The K-distribution has been a popular model for X-band maritime surveillance radar clutter [24, 25].

The second comparison fit is provided by the Weibull distribution [26]. A random variable $\mathcal{W}$ has a Weibull distribution with shape parameter σ and scale parameter λ if its density is

$$f_{\mathcal{W}}(t) = \frac{\sigma}{\lambda}\left(\frac{t}{\lambda}\right)^{\sigma-1} e^{-\left(\frac{t}{\lambda}\right)^{\sigma}}, \tag{11}$$

which also supports the non-negative real line. The Weibull distribution has been found to be a suitable model for some radar data sets [27], including the DST Group's Ingara radar data. In particular, vertically polarised high resolution maritime surveillance radar clutter can be well modelled by the Weibull distribution, as documented in [12].

The data used in the following analysis have been acquired with DST Group's Ingara radar. This radar operated in a circular spotlight mode, emulating a typical maritime surveillance radar. The data used for the purposes of modelling here was acquired during a trial in August 2004. During the data gathering exercise, the radar surveyed the same ocean patch at different azimuth angles, operating at 10.1 GHz with a 20 µs compressed pulse width, with a range resolution of 0.75 m. The fitting of the Pareto Type II model to the Ingara data is described in [5]. Here the focus will be restricted to data acquired with horizonal transmit and receive polarisation, since in this case the data are heavy tailed, and the Pareto model is most suitable [2].

Two particular data sets will be considered here; they are designated run 34 683 and run 34 690, which have been investigated extensively. As discussed in the latter, these data sets were collected from scans of the Southern Ocean, on August 16, 2004, at around 10:52 am local time. These runs consist of 1024 range compressed samples of between 800 and 900 pulses, in 5° azimuth angle increments. Run 34 683 was collected at an incidence angle of 51.3°, at an altitude of approximately 2314 m. In the case of run 34 690, the incidence angle was 67.2°, at an altitude of roughly 1353 m. The wind speed, at the mid-data collection time on the trial day, was reported to be 7.1 m/s, in a direction of 47°, with a wave height of 2.4 m in a direction of 211°. The upwind direction was 227°, downwind at 47°, while the cross wind directions were 137° and 317°, respectively. Further details of the data and its analysis can be found in [8–10].

Table 1 shows the resultant parameter estimates, when the Pareto, K, Weibull and Burr distributions are fitted to the Ingara data. The first nineteen lines in the table show results for fitting to data set run 34 683, at the given azimuth angles. The final four lines record similar results for run

Table 1. Maximum likelihood parameter estimates of the various statistical models fitted to Ingara data sets. The first nineteen lines correspond to run 34 683 (azimuth 0° to 355°, while the last four are based upon run 34 690, at azimuth angles of 45°, 135°, 225° and 355°.

Azimuth	Pareto α	Pareto β	K c	K ν	Weibull λ	Weibull σ	Burr α	Burr β	Burr κ
0	5.714507965	0.013092894	84.17569766	4.906478507	0.002626984	0.896229357	5.312139208	0.011143052	1.013252807
5	5.592745076	0.012751119	82.89108337	4.755727574	0.002620449	0.893301844	4.665284084	0.009113872	1.021606413
10	4.20927818	0.010011378	67.19255229	3.496033486	0.002868966	0.858924093	4.050591542	0.009128596	1.008064034
25	5.402808624	0.016447941	70.43332782	4.619707226	0.003520199	0.889518989	4.993181923	0.013985338	1.012853147
45	3.719335324	0.012905678	50.76561664	3.02286036	0.004287094	0.841769643	3.845732515	0.01394197	0.993137715
60	3.16698186	0.01256309	42.24442194	2.535297662	0.005093407	0.817257474	3.392867185	0.01483835	0.984487494
90	4.057710669	0.016251336	49.58529281	3.239367241	0.004844893	0.852622735	4.658816509	0.021765264	0.975355423
100	3.958318927	0.015754377	49.3784454	3.216327863	0.00484964	0.850298184	4.152088657	0.017508719	0.990741085
135	7.198688347	0.02265872	82.58786574	6.225599756	0.003502345	0.916524397	7.076885612	0.022013966	1.00167794
150	4.837311559	0.01146727	73.99748464	4.072468725	0.002788209	0.876988252	4.592057972	0.010229627	1.009266136
180	4.51600883	0.014456084	60.37011068	3.724901897	0.003803936	0.867197408	4.600605146	0.015045765	0.996667402
190	4.903113972	0.02088792	55.42390883	4.094952732	0.0049975	0.875757309	4.675460853	0.018915962	1.008448625
225	4.724046998	0.044630145	35.99470865	3.863402918	0.011124652	0.871609417	5.050578389	0.050665814	0.988772595
255	5.289354607	0.057518708	36.53869103	4.461416571	0.012599969	0.886428038	5.131624329	0.054388258	1.004964803
270	5.999584913	0.060914077	40.73504998	5.04323166	0.011540632	0.899324453	6.177461881	0.064080882	0.995915244
280	6.92006662	0.061043571	48.13933298	5.966405485	0.009861131	0.912912134	6.721505343	0.058097901	1.003795423
325	4.446297104	0.016661269	55.09058417	3.647056579	0.004465652	0.864702358	4.521220238	0.017268376	0.996957545
350	5.071878959	0.011573571	77.78086767	4.282307187	0.002663151	0.882965401	4.731170568	0.01003559	1.01104043
355	5.229213919	0.0125478	77.46161373	4.435467915	0.002787208	0.886140855	4.902818485	0.010933323	1.010854296
45	3.27556654	0.001838552	116.3948754	2.696582369	0.000718704	0.817422628	3.299415698	0.001778496	1.003974284
135	3.719145438	0.001870769	135.2830377	3.118514816	0.00062491	0.83883413	3.762458903	0.001908812	0.999743257
225	2.500088338	0.003433667	60.40378706	2.011799389	0.001910291	0.76475364	2.238755733	0.002387426	1.034561965
355	3.465317914	0.002905296	99.16402142	2.859673879	0.001057063	0.828922105	4.211096162	0.004436571	0.970831225

34 690, but at azimuth angles in approximately the down wind, cross wind and up wind directions. All parameter estimates were acquired with Matlab's inbuilt MLE fit procedure. It is interesting to note that in the case of the Burr fit to the data, the second shape parameter κ is always close to unity, but offset by a fraction. In addition to this, one observes that the estimate of parameter β in the Burr model is always small.

Next examples of the fits of the various models are provided by plotting empirical cumulative distribution functions (ECDFs) of the data and also the fitted distributional models. These examples are at azimuth angles of 45°, 135° and 225° for run 34 683. In the case of run 34 690, only results at azimuth angles of 135° and 225° are provided for brevity. To clarify the resultant fits, the lower and upper tail regions of the fit will be emphasised.

Figures 1 and 2 show the lower and upper tail fits for the case of 45° azimuth, for run 34 683. It is clear that in this case the K and Weibull distributional fits are not suitable. Here the Pareto and Burr fits are somewhat similar; there are regions where the Pareto is slightly better, followed by regions where the Burr fit is an improvement.

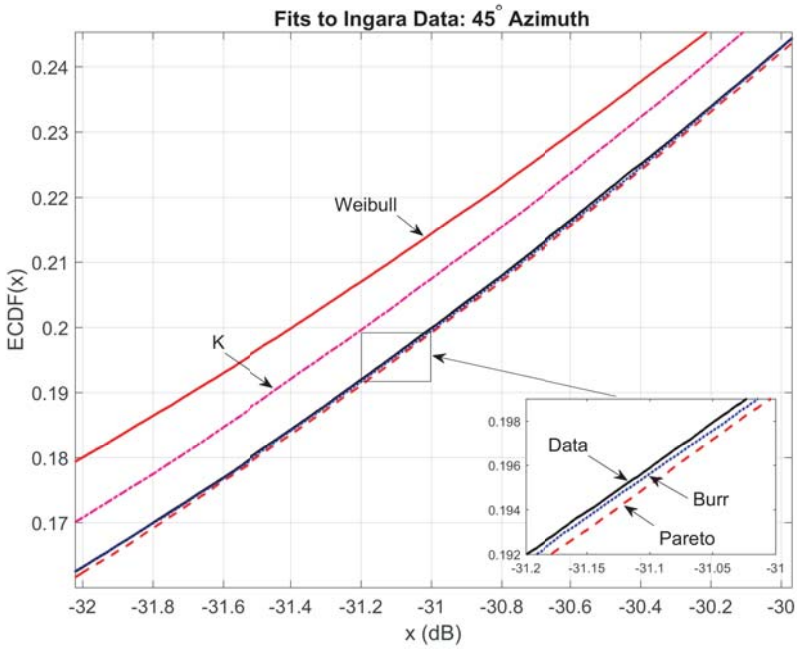

Figure 1. Fits in the lower tail region, at azimuth 45° for run 34 683.

Next the case of 135° azimuth is examined, for run 34 683, with Figure 3 an example of fits in the lower tail region, and Figure 4 for the upper tail region. As in the previous azimuth case, the Weibull fit is inappropriate, while the K-distributional fit is not as good as the Pareto and Burr. In these figures it is evident that the Burr fit can be tighter than the Pareto Type II fit, but there tends to be regions where this can vary.

As a final example of fits to run 34 683, the azimuth of 225° is considered next, which is the direction closest to upwind, corresponding to the spikiest data available. Figure 5 is for the lower tail region, while Figure 6 is for the upper tail region. These figures illustrate that the Burr model can give a much tighter fit than the Pareto Type II, in very spiky clutter.

Next distributional fits to run 34 690 are examined. In the first instance, the case of 135° azimuth is examined, with Figure 7 for the lower tail region and Figure 8 for the upper tail region. In the lower tail region the Burr model provides a slight improvement, while in the upper tail region, the Pareto Type II model is slightly better.

To complete the analysis, fits to the case of 225° are examined for run 34 690, with Figure 9 showing distributional fits in the lower tail region. Here the Burr distribution is a better fit. Figure 10 shows

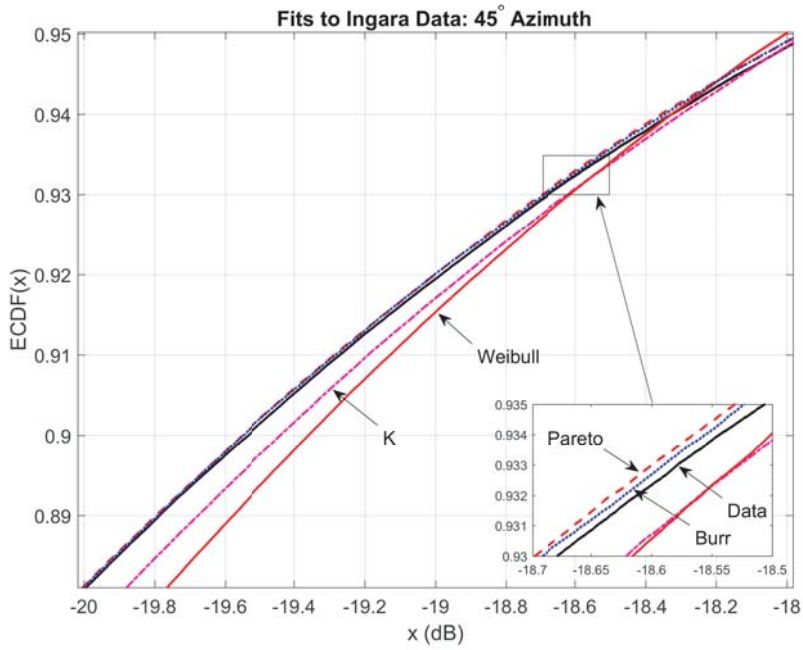

Figure 2. Fits in the upper tail region, at 45° azimuth, for run 34 683.

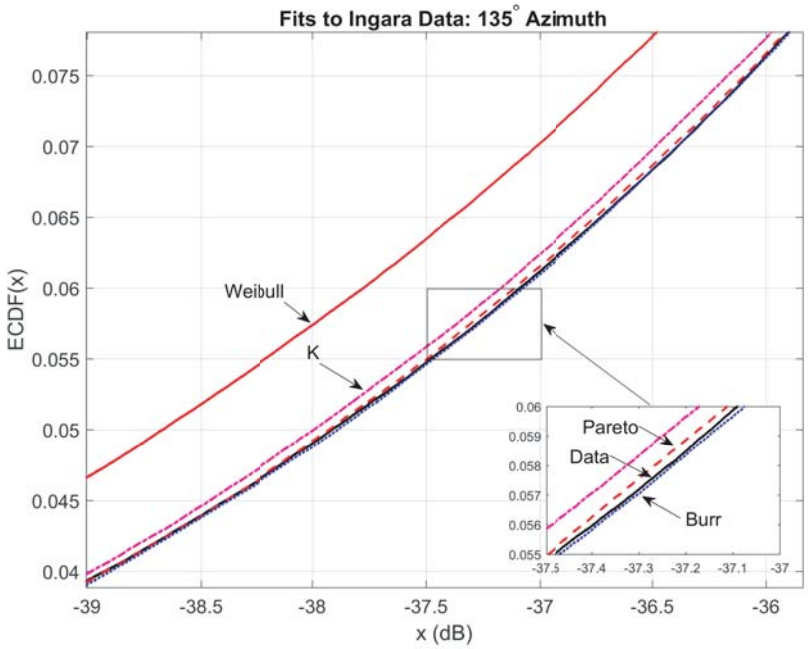

Figure 3. Lower tail fits in the case of 135° azimuth, for run 34 683.

the fits in the upper tail region. The Burr distribution provides a slightly better fit than the Pareto model.

Based upon these results it is clear that the Burr distribution can provide a better fit to DST Group's Ingara radar clutter. Hence there is merit in the examination of non-coherent detection processes for operation in Burr distributed clutter. This analysis begins in Section 4.

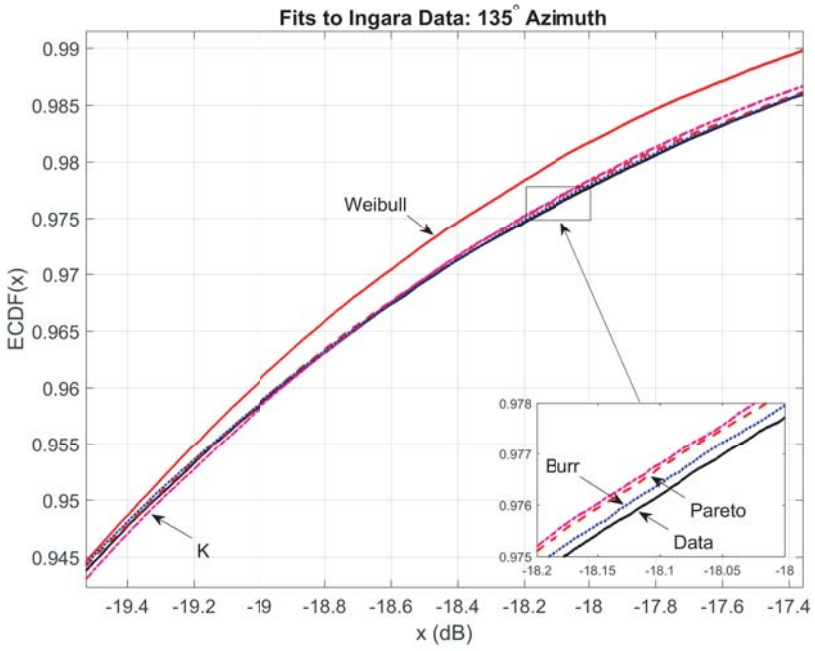

Figure 4. Upper tail fits in the case of 135° azimuth, for run 34 683.

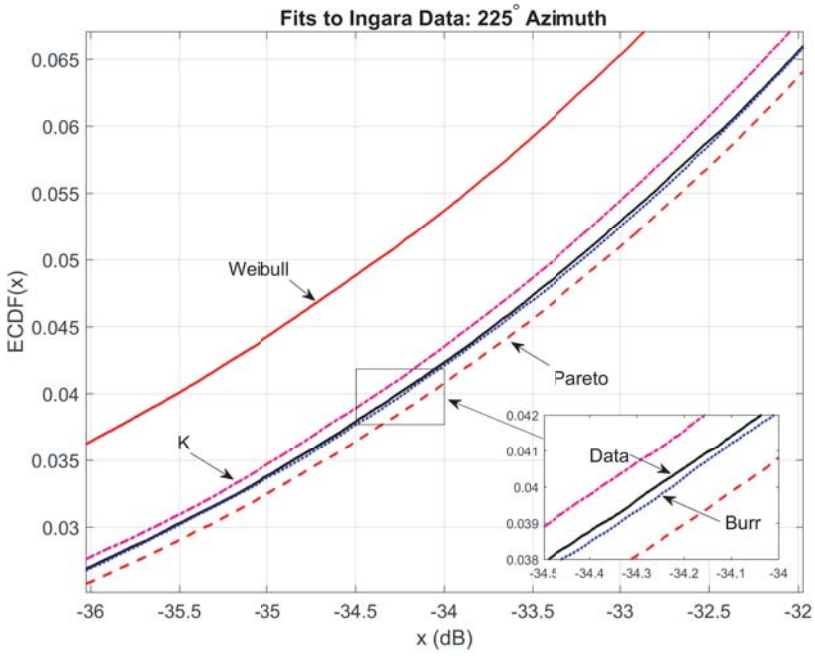

Figure 5. Fits at an azimuth of 225° in the lower tail region, for run 34 683.

4. DEVELOPMENT OF NON-COHERENT DETECTORS

The development of non-coherent sliding window detectors, for operation in Burr distributed clutter, is now examined. A useful guide on such detectors is [1], while some more recent examples of development of such detectors include [28–37]. These detectors assume the existence of a series of independent

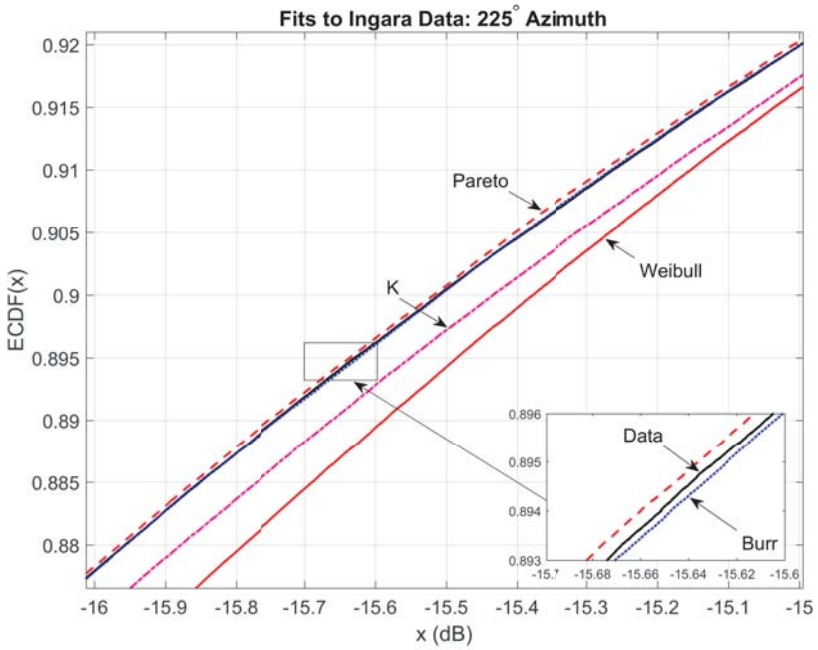

Figure 6. Upper tail fits at azimuth of 225°, for run 34 683.

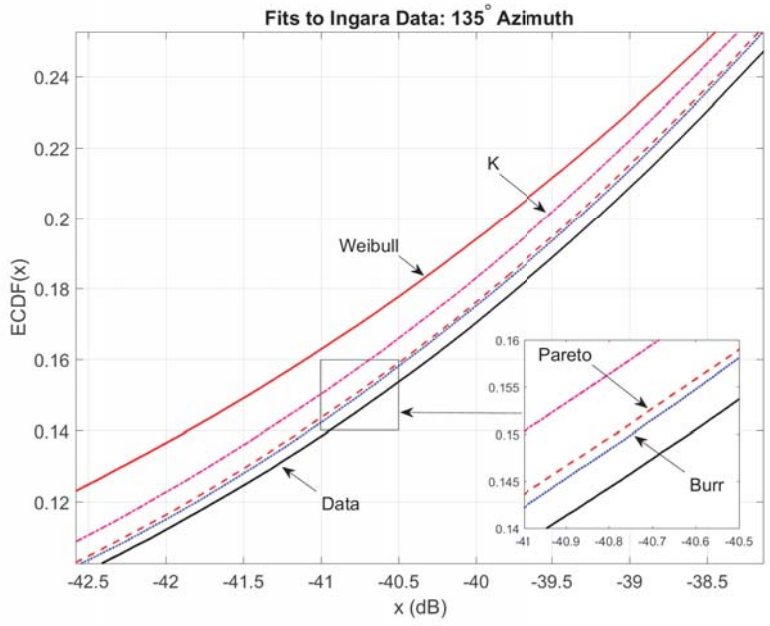

Figure 7. Lower tail fits at 135° azimuth, for run 34 690.

and identically distributed clutter measurements, denoted $Z_1, Z_2, \ldots, Z_N$, which are referred to as the clutter range profile (CRP). A CUT is taken, which is denoted Z_0 and is separated from the clutter measurements using a series of guard cells. These are used to mitigate the effects of a range spread target [18]. A function f is applied subsequently to the CRP to produce a single measurement of the clutter level. A multiplicative normalisation constant $\tau > 0$ is then applied to f, in such a way that in homogeneous clutter returns the Pfa can be set, hopefully independently of the clutter power. As has

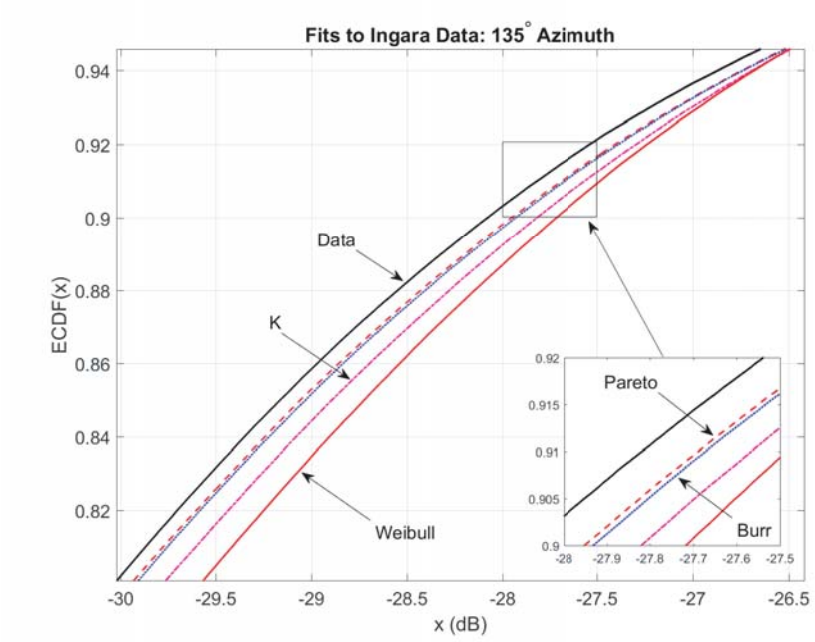

Figure 8. Upper tail fits at 135° azimuth, for run 34 690.

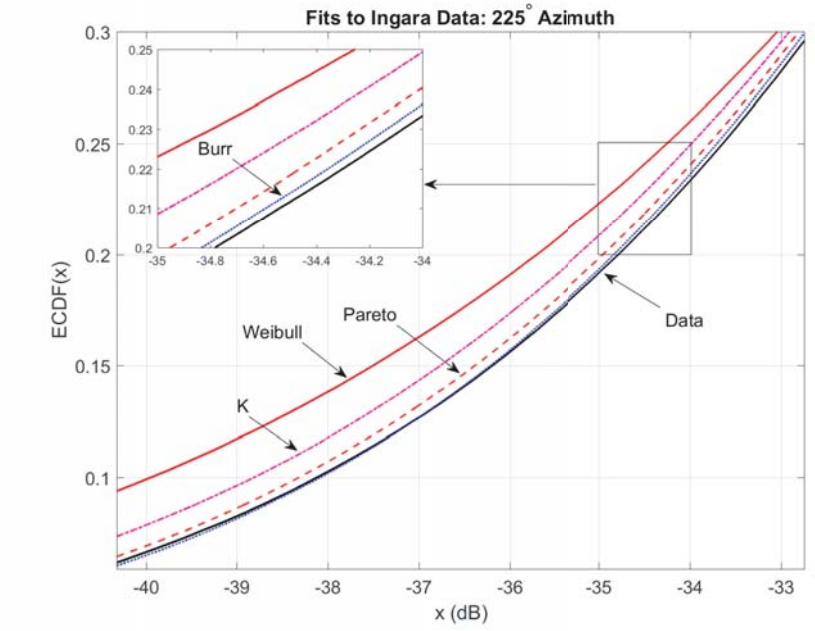

Figure 9. Lower tail fits at 225° azimuth, for run 34 690.

been discussed in [19], the scale invariance of f will yield detectors with the CFAR property, provided that the clutter model is also scale invariant. It is also shown in the latter that sliding window detection processes, with the CFAR property, can be derived in the case where the clutter is modelled by scale and power invariant distributions.

To formulate this in the language of statistical hypothesis testing, suppose that H_0 is the hypothesis that the CUT does not contain a target, and let H_1 be the alternative hypothesis that the CUT contains

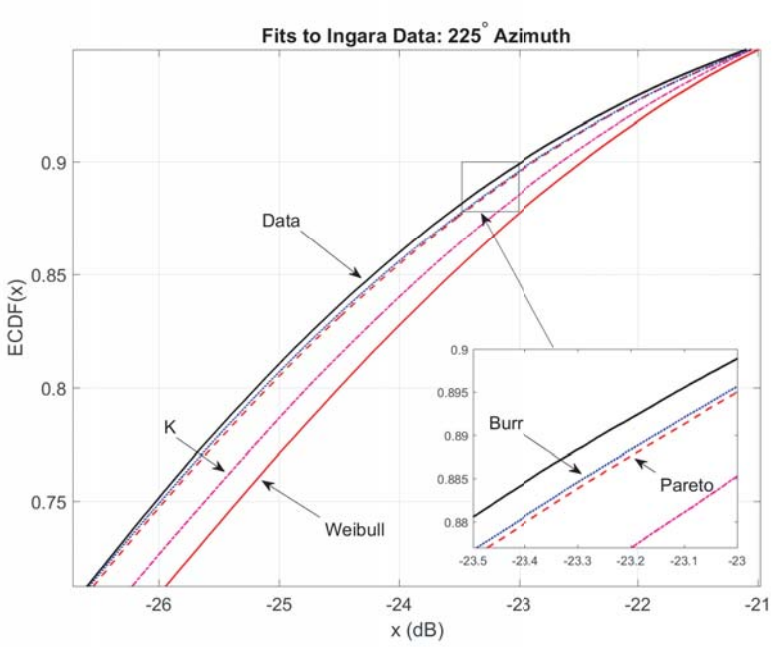

Figure 10. Upper tail fits at 225° azimuth, for run 34 690.

a target embedded within clutter. Then the test can be written

$$Z_0 \underset{H_0}{\overset{H_1}{\gtrless}} \tau f(Z_1, Z_2, \ldots, Z_N), \tag{12}$$

where the notation employed in Equation (12) means that H_0 is rejected only in the case where $Z_0 > \tau f(Z_1, Z_2, \ldots, Z_N)$. If a test in the form of Equation (12) can be constructed such that its Pfa given by

$$\mathrm{P_{FA}} = \mathbb{P}(Z_0 > \tau f(Z_1, Z_2, \ldots, Z_N) | H_0) \tag{13}$$

does not vary with the clutter power, then the test of Equation (12) is referred to as having the CFAR property. This is equivalent to the condition that τ can be determined from Equation (13) in such a way that it does not depend on an unknown clutter parameter [2]. In the classical case where the clutter is modelled by exponential random variables it is well known that Equation (12) will achieve the CFAR property provided that f is a scale-invariant function [18]. When detectors of the form (12) are applied to the operation in other clutter environments, there is often a loss of the CFAR property. As an example, in the Weibull clutter case, a detector of the form (12) is only CFAR with respect to the Weibull scale parameter [12]. This situation is replicated for the Pareto Type I and II cases, as illustrated in [15] and [38]. Another issue with the application of Equation (12) to non-exponentially distributed clutter environments is inherent difficulty in determining a closed form expression for the Pfa as a function of the threshold multiplier τ. To illustrate this, consider the case under investigation in this paper, where the members of the CRP have Burr distributions. Then with the selection of f as a sum, producing a cell-averaging detector, it will be necessary to determine the distribution of a sum of independent and identically distributed Burr random variables, which does not have a closed form. Although a simulation strategy can be utilised to determine τ, the issue is that this can introduce a huge computational burden, since very large sample sizes will be required for Pfas of interest.

In order to circumvent these issues and also in an attempt to introduce the full CFAR property for such detectors operating in modern clutter environments, [11] and [12] introduced a transformation approach. This technique transforms detectors of the form (12), for operation in non-exponentially distributed clutter, while preserving Equation (13) for the pre-transformed detector operating in exponentially distributed clutter. This procedure eliminated the need for a simulation-based approach for determination of the threshold multiplier. In the Pareto Type I case, the transformation approach

resulted in the generation of non-coherent detectors with the CFAR property with respect to the distributional shape parameter. Unfortunately, these transformed decision rules required *a priori* knowledge of the Pareto scale parameter.

To introduce the main result from [12] and in the current context, suppose that Z has a Burr distribution with Equation (1) as its distribution function. Define a transfer function

$$H(t) = F_Z^{-1}(1 - e^{-t}) = \left(\beta\left(e^{\frac{t}{\alpha}} - 1\right)\right)^{\frac{1}{\kappa}} \tag{14}$$

where Equation (6) has been utilised. A direct calculation demonstrates that the inverse of H is

$$H^{-1}(t) = \frac{1}{\alpha}\log\left(\frac{\beta}{\beta + t^{\kappa}}\right). \tag{15}$$

Then the decision rule

$$Z_0 \underset{H_0}{\overset{H_1}{\gtrless}} H\left(\tau f\left(H^{-1}(Z_1), \ldots, H^{-1}(Z_N)\right)\right) \tag{16}$$

is a transformed version of Equation (12), for operation in Burr distributed clutter, which has τ set via Equation (13) for the exponentially distributed clutter case.

To illustrate this, with the selection of f as a sum, Equation (16) is reduced to

$$Z_0 \underset{H_0}{\overset{H_1}{\gtrless}} \left(\beta\left[\prod_{j=1}^{N}\left(1 + \frac{Z_j^{\kappa}}{\beta}\right)^{\tau} - 1\right]\right)^{\frac{1}{\kappa}}, \tag{17}$$

whose threshold multiplier τ is given by

$$\tau = {\mathrm{P_{FA}}}^{-\frac{1}{N}} - 1. \tag{18}$$

The latter relationship is the Pfa of Equation (12), with f selected to be a sum, when operating in exponentially distributed clutter. Similarly, when f is selected to be the kth OS of the CRP, the detector (16) becomes

$$Z_0 \underset{H_0}{\overset{H_1}{\gtrless}} \left(\beta\left[\left(1 + \frac{Z_{(k)}^{\kappa}}{\beta}\right)^{\tau} - 1\right]\right)^{\frac{1}{\kappa}}, \tag{19}$$

with τ set via numerical inversion of

$$\mathrm{P_{FA}} = \frac{N!}{(N-k)!}\frac{\Gamma(N - k + \tau + 1)}{\Gamma(N + \tau + 1)}. \tag{20}$$

It is important to observe that these transformed detectors are CFAR with respect to the Burr shape parameter α but require *a priori* knowledge of the second shape parameter κ and the Burr scale parameter β.

In view of Equation (7) and with reference to the analysis of invariant decision rules in [19], it is clear that the Burr distribution falls into the class of scale and power invariant models, when α is assumed known. Hence it is possible to construct detectors which are CFAR with respect to κ and β. As a simple example, one can consider the Weber-Haykin detector

$$Z_0 \underset{H_0}{\overset{H_1}{\gtrless}} Z_{(1)}^{1-\tau} Z_{(k)}^{\tau}, \tag{21}$$

where the lower OS has been selected to be the minimum to facilitate the derivation of the Pfa as a function of τ. It is assumed that the index of the second OS in Equation (21) is such that $2 \leq k \leq N$. The following lemma provides an expression for its Pfa:

Lemma 4.1 *The Pfa of the Weber-Haykin detector* (21)*, operating in Burr distributed clutter, is given by*

$$\begin{aligned}\mathrm{P_{FA}} \;=\; & N(k-1)\binom{N-1}{k-1}\int_0^1\int_0^1 \phi^{N-1}(1-\psi)^{k-2}\psi^{N-k} \\ & \times\left[1 + \left[\phi^{-\alpha^{-1}} - 1\right]^{1-\tau}\left[(\psi\phi)^{-\alpha^{-1}} - 1\right]^{\tau}\right]^{-\alpha} d\phi d\psi.\end{aligned} \tag{22}$$

The proof of Lemma in Equation 4.1 is now provided. Based upon Equation (7) one may write $Z_j = \Phi_1 W_j^{\Phi_2}$ where $\Phi_1 = \beta^{\frac{1}{\kappa}}$ and $\Phi_2 = \frac{1}{\kappa}$, which expresses the Burr model in terms of scale and power transformations. Here W_j has a Pareto Type II distribution, with shape parameter α and scale parameter equal to unity. Then it is not difficult to show that the Pfa is equivalent to

$$\mathrm{P_{FA}} = \mathbb{P}(W_0 < W_{(1)}^{1-\tau} W_{(k)}^{\tau}) \tag{23}$$

where W_0, which is equivalent to the CUT under H_0, also has the same Pareto Type II distribution as W_j. It is explained in [2] that one may write

$$W_j \stackrel{d}{=} e^{\alpha^{-1} X_j} - 1 \tag{24}$$

where X_j has an exponential distribution with mean unity. This relationship allows the Pareto Type II model to be expressed in terms of a transformation of a standard exponential model and is referred to as the Pareto-Exponential Duality Property. Since this also applies to the CUT statistic W_0, the Pfa in Equation (23) is equivalent to

$$\mathrm{P_{FA}} = \mathbb{P}\left(\log W_0 > (1-\tau)\log(e^{\alpha^{-1} X_{(1)}} - 1) + \tau \log(e^{\alpha^{-1} X_{(k)}} - 1) \right), \tag{25}$$

where $X_{(k)}$ is the kth OS of the exponentially distributed random variables X_j. This result follows since expression (24) extends to the sample order statistics. Noting that the minimum of an exponentially distributed sample with unit mean also has an exponential distribution, but with parameter N, and it is followed by conditional probability that

$$\begin{aligned} \mathrm{P_{FA}} \;=\; & \int_0^{\infty} N e^{-Nt} \mathbb{P}\left[\log W_0 > (1-\tau)\log\left(e^{\alpha^{-1} t} - 1\right) \right. \\ & \left. + \tau \log\left(e^{\alpha^{-1} X_{(k)}} - 1\right) \Big| X_{(1)} = t \right] dt. \end{aligned} \tag{26}$$

For brevity, define a random variable $Y_{(k)} = X_{(k)} | \{X_{(1)} = t\}$. It is shown in [16] that such a random variable can be related to exponential random variables. In particular $Y_{(k)} \stackrel{d}{=} Q_{(k)} + t$ where $Q_{(k)}$ is the $(k-1)$th OS of a series of $N-1$ independent and identically distributed exponential random variables with unity mean. Therefore, it follows that the density of $Y_{(k)}$ is $f_{Y_{(k)}}(y) = f_{Q_{(k)}}(y-t)$ provided $y \geq t$ and zero otherwise. It is shown in [2] that the latter density is

$$f_{Q_{(k)}}(w) = (k-1)\binom{N-1}{k-1} \left(1 - e^{-w}\right)^{k-2} e^{-w(N-k+1)}. \tag{27}$$

Consequently,

$$\begin{aligned} \mathrm{P_{FA}} \;&=\; \int_0^{\infty} N e^{-Nt} \int_{y=t}^{\infty} \mathbb{P}\left[W_0 > e^{(1-\tau)\log\left[e^{\alpha^{-1} t} - 1\right] + \tau \log\left[e^{\alpha^{-1} t} - 1\right]} \right] f_{Q_{(k)}}(y-t) dy dt \\ &=\; \int_0^{\infty} N e^{-Nt} \int_{y=t}^{\infty} \left[1 + \left[e^{\alpha^{-1} t} - 1\right]^{1-\tau} \left[e^{\alpha^{-1} y} - 1\right]^{\tau} \right]^{-\alpha} f_{Q_{(k)}}(y-t) dy dt, \end{aligned} \tag{28}$$

where the fact that the CUT has complementary distribution function $\mathbb{P}(W_0 > \phi) = (\phi+1)^{-\alpha}$ has been applied. Finally, by applying Equations (27) to (28), and applying the transformations $z = y - t$, followed by $\phi = e^{-t}$ and then $\psi = e^{-z}$, the desired expression for the Pfa is obtained, completing the proof.

Based upon Lemma 4.1 it is clear that the Weber-Haykin detector (21) is CFAR with respect to κ and β, but requires *a priori* knowledge of α.

Although it is reported in [15] that direct adaptation of the decision rule in Equation (12) to non-exponentially distributed clutter environments is not the most effective technique to produce sliding window detectors, one can nonetheless derive decision rules based upon this approach. Here only two OS detectors will be examined. The first results from the selection of f as the kth OS, with decision rule

$$Z_0 \underset{H_0}{\overset{H_1}{\gtrless}} \tau Z_{(k)}. \tag{29}$$

The Pfa, in the Burr distributed clutter case, is given by the following result:

Lemma 4.2 *The Pfa of Equation* (29) *is*

$$\mathrm{P_{FA}} = \frac{N!}{(N-k)!(k-1)!}\int_0^1 \omega^{N-k}(1-\omega)^{k-1}\left[1+\tau^{\kappa}\left(\omega^{-\frac{1}{\alpha}}\right)\right]^{-\alpha} d\omega. \tag{30}$$

In order to prove this result, note that under H_0 the CUT has the equivalent distribution

$$Z_0 \overset{d}{=} \left[\beta\left(e^{\alpha^{-1}X_0}-1\right)\right]^{\frac{1}{\kappa}}, \tag{31}$$

where X_0 has an exponential distribution with unity mean, and so by applying Equation (31), together with Equations (8) and (9), one obtains

$$\begin{aligned}\mathrm{P_{FA}} &= \mathbb{P}\left(e^{\alpha^{-1}X_0}-1 > \tau^{\kappa}\left(W_k^{-\frac{1}{\alpha}}-1\right)\right)\\ &= \int_0^1 f_{W_k}(w)\mathbb{P}\left(X_0 > \alpha\log\left(1+\tau^{\kappa}\left(w^{-\frac{1}{\alpha}}-1\right)\right)\right)dw\\ &= \frac{N!}{(N-k)!(k-1)!}\int_0^1 w^{N-k}(1-w)^{k-1}\left(1+\tau^{\kappa}\left(w^{-\frac{1}{\alpha}}-1\right)\right)^{-\alpha},\end{aligned} \tag{32}$$

which completes the proof. Observe that Lemma 4.2 implies Equation (29) is CFAR with respect to β only.

As an alternative to Equation (29), one can examine the effects of raising the OS to the power of τ, instead of it being a multiplicative factor. Hence one can examine the detector

$$Z_0 \underset{H_0}{\overset{H_1}{\gtrless}} Z_{(k)}^{\tau}. \tag{33}$$

Its Pfa is given by the following result:

Lemma 4.3 *The Pfa of Equation* (33)*, operating in Burr distributed clutter, is*

$$\mathrm{P_{FA}} = \frac{N!}{(N-k)!(k-1)!}\int_0^1 \omega^{N-k}(1-\omega)^{k-1}\left[1+\beta^{\tau-1}\left(\omega^{-\frac{1}{\alpha}}-1\right)^{\tau}\right]^{-\alpha} d\omega. \tag{34}$$

The proof of this result is similar to that of Lemma 4.2 and is thus omitted. Again, note that Lemma 4.3 implies that the detector (33) is CFAR only with respect to κ.

Thus a series of five non-coherent detectors has been introduced, with varying degrees of the CFAR property. The next section examines the performance of these five decision rules.

5. PERFORMANCE ANALYSIS

Throughout the following the length of the CRP has been set to $N = 32$ with the Pfa equal to 10^{-4}. All OS indices have been selected to be $k = N-2 = 30$. This is so that detectors based upon this OS are able to manage up to two interfering targets in the CRP. Clutter is simulated through Equation (7), with the Burr distributional parameters $\alpha = 5.050578389, \beta = 0.050665814$ and $\kappa = 0.988772595$. These choices correspond to the fits acquired from run 34 683, at an azimuth angle of 225° (see Table 1). If a decision rule requires *a priori* knowledge of a particular clutter parameter, then this value is applied directly. Monte Carlo sampling, with 10^6 runs, is used to estimate each probability of detection (Pd) for every SCR. The expression for the latter is facilitated by application of Equation (5). In all cases a Gaussian target model has been used in the complex domain, together with a complex clutter component, for the CUT. An upper bound is also provided, which has been produced by construction of a linear threshold detector. This has a decision rule given by

$$Z_0 \underset{H_0}{\overset{H_1}{\gtrless}} \left(\beta\left[\mathrm{P_{FA}}^{-\frac{1}{\alpha}}-1\right]\right)^{\frac{1}{\kappa}}, \tag{35}$$

which has been derived through calculation of the corresponding Pfa.

The first performance example to be considered can be found in Figure 11, which shows the performance of the detectors operating in homogeneous clutter. Throughout the following the

detector (17) is labelled as TCA (transformed cell averager), Equation (19) referred to as TOS (transformed OS), and Equation (21) labelled WH (for Weber Haykin). The detector (29) is labelled CD (for classical detector) while Equation (33) is marked POW (power). As can be observed from Figure 11, the detector (33) matches the performance of the fixed threshold detector, while the detector (29) is slightly inferior. The transformed detectors perform slightly worse than Equation (29), while the Weber-Haykin detector has the worst performance. The latter can be explained by the fact that this detector is CFAR with respect to two clutter parameters. The best performing detector, namely Equation (33), requires *a priori* knowledge of α and β, and is only CFAR with respect to κ. Hence it appears that detectors with more critical information assumed, in terms of clutter parameters, tend to have better performance than decision rules which are CFAR.

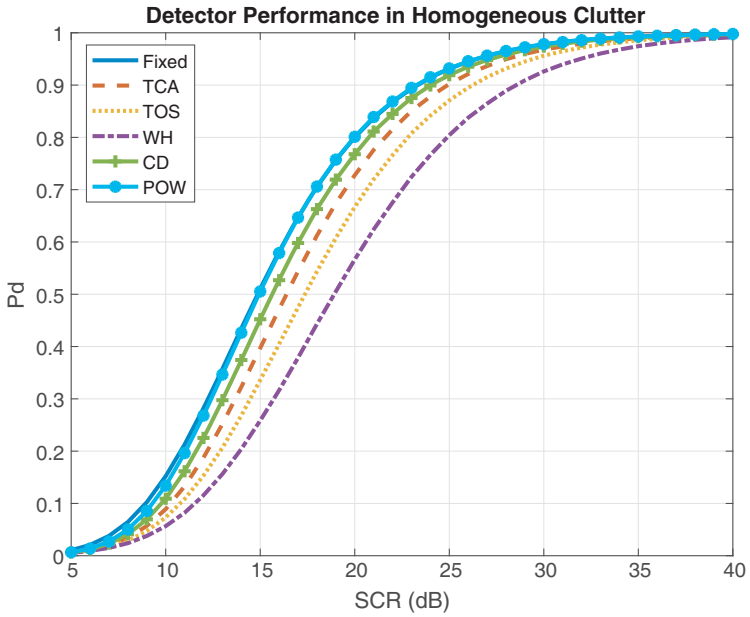

Figure 11. Detection performance in homogeneous Burr distributed clutter.

Next the effects of two independent interfering Gaussian targets in the CRP are examined, which can arise from a range spread target in the CUT [18]. Figure 12 shows the case where the interfering targets have SCR of 1 dB. Here one can observe a slight change in detection performance of the five decision rules. Figure 13 illustrates the consequence of increasing the interference to one target with SCR of 10 dB and a second with SCR of 20 dB. Finally, Figure 14 demonstrates the effect on performance when both interfering targets have SCR of 30 dB. These results show that the transformed cell averaging detector (17) suffers the most in the presence of increasing interference. The transformed OS detector (19) and the Weber-Haykin detector (21) tend to perform similarly in the presence of increasing interference. The detector with the greatest resilience to interference is Equation (33), followed by Equation (29).

The next stage of performance analysis involves examining the Pfa of each detector during clutter power transitions. In this case, the resultant Pfa is estimated, when the CRP is saturated sequentially by higher powered clutter returns [18]. Such an analysis informs one on the resilience of a detector in terms of preserving the design Pfa when the clutter is acquired from different regions. To illustrate this, the resultant Pfa is estimated as a function of the number of higher powered clutter returns. Interpreting clutter power as mean squared, one can apply Equation (5) with $r = 2$ to determine a suitable set of parameters for higher powered clutter at a specified dB level. For simplicity, it is assumed that the Burr parameters β and κ are fixed. Then for an x dB clutter power increase, it can be shown that one must determine an α' via the solution to

$$\alpha' \mathcal{B}\left(\alpha' - \frac{2}{\kappa}, \frac{2}{\kappa} + 1\right) - 10\alpha \log_{10}(x) \mathcal{B}\left(\alpha - \frac{2}{\kappa}, \frac{2}{\kappa} + 1\right) = 0, \tag{36}$$

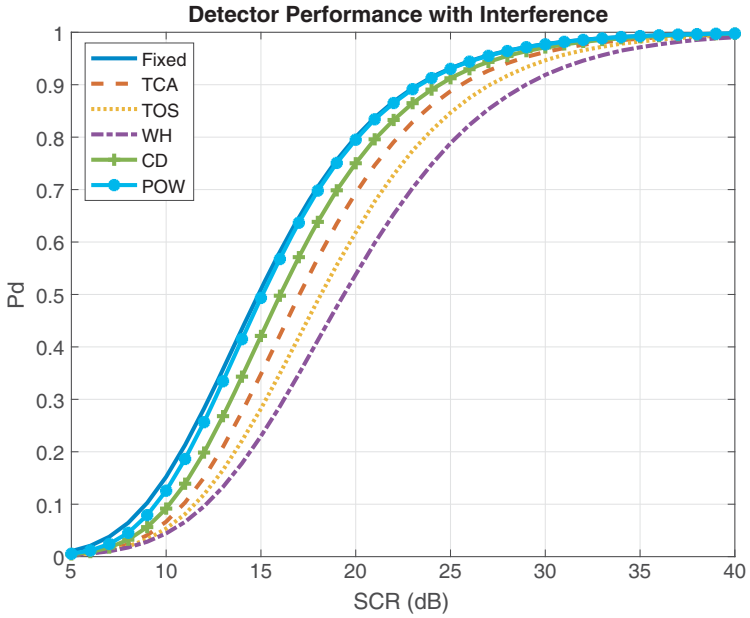

Figure 12. Performance when the CRP contains two independent interfering targets with SCR of 1 dB.

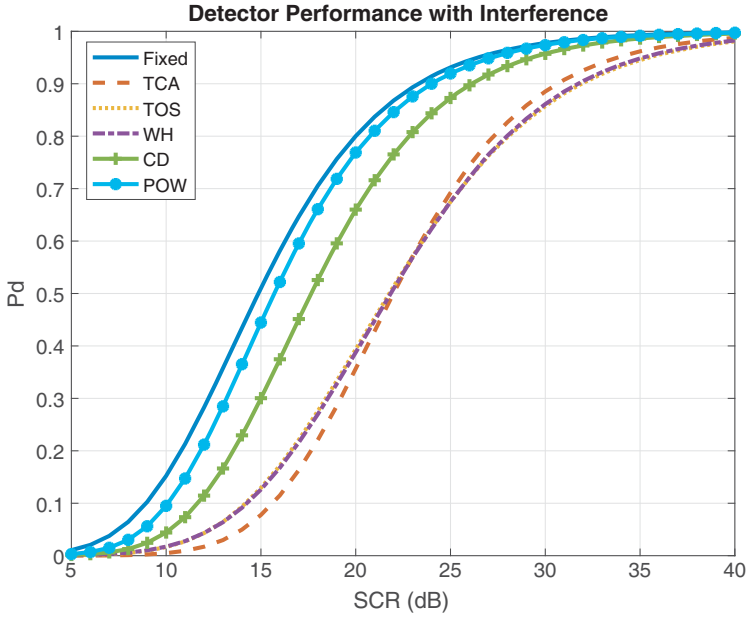

Figure 13. Performance in the presence of one 10 dB and one 20 dB interfering target in the CRP.

where $\mathcal{B}$ is the beta function, α' the Burr shape parameter in the higher power clutter, and α the Burr shape parameter in the lower powered clutter. As is the common practice in such analyses, when the mid-point of the CRP is saturated with higher powered clutter, the CUT is then assumed to also be saturated with higher power clutter. Since the threshold multiplier is set in the lower power clutter region, this results in a jump in the plots of estimated Pfa.

Figure 15 shows the results when the five detectors are subjected to a 2 dB clutter power increase. As the number of higher power clutter cells is increased, the detector (33) maintains the design Pfa with less error than the other decision rules, which reduce the resultant Pfa. Once the CUT is saturated with higher power clutter, the two transformed detectors have the least increase in resultant Pfa.

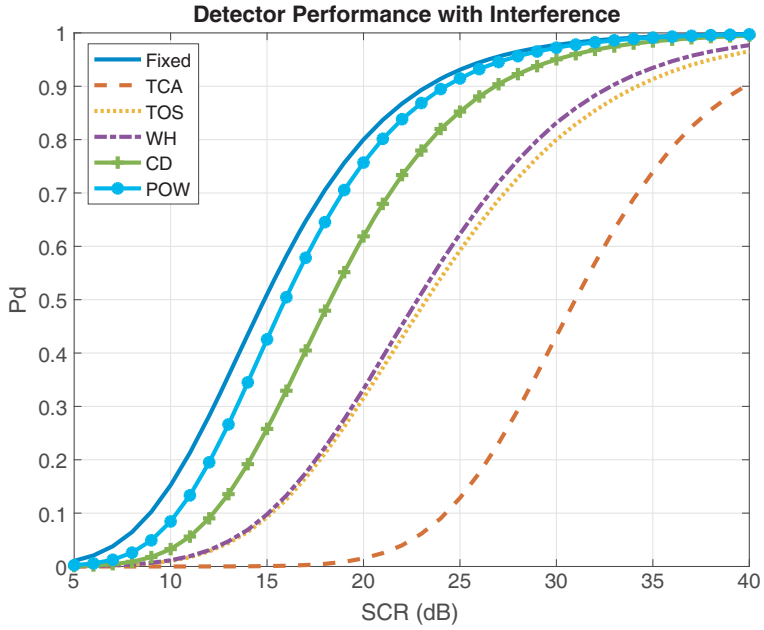

Figure 14. Performance in the presence of strong interference in the CRP, provided by two 30 dB interfering targets.

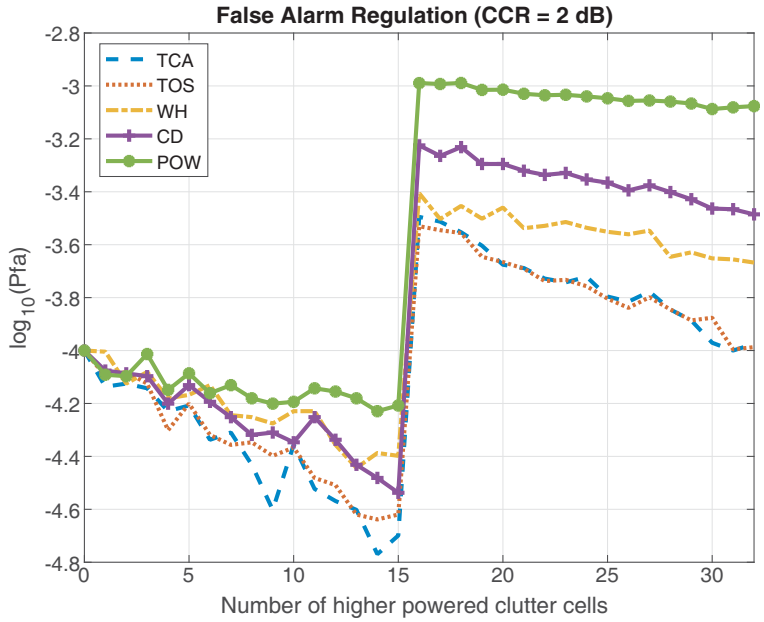

Figure 15. Effects of a 2 dB clutter power increase on the resultant Pfa, where the design Pfa is 10^{-4} and $N = 32$.

To complete the numerical analysis, the five decision rules were run directly on the Ingara data set used as a basis for the simulated studies. Each detector was implemented as a sliding window process, where two guard cells were applied to both sides of the CUT. As in the preceding analysis a Gaussian target was inserted into the CUT. The data set consisted of 840, 704 measurements and hence with a CRP of 32 and 4 guard cells which permitted a Monte Carlo sampling size of 840, 667. Figure 16 shows the performance of the decision rules. Compared with Figure 11, one can see that there is a slight variation in performance. As an example, in Figure 11 the Weber-Haykin detector has a nominal Pd of

0.5 at roughly 18 dB SCR. In Figure 16, this occurs at around 16 dB. Similar effects can be noted for the other decision rules. To explain this, the resultant Pfa of each detector, when running on the Ingara data set, was also calculated. These results are shown in Table 2. As can be observed, each decision rule experiences a deviation from the design Pfa, explaining the discrepancy between the figures. This is attributable to the fact that the real data is correlated and inhomogeneous, while the detectors have been designed for operation in homogeneous independent clutter. It is interesting to note that the detector (33), which has a very small deviation from the design Pfa, performs comparably to the same detector running in the independent simulated clutter case.

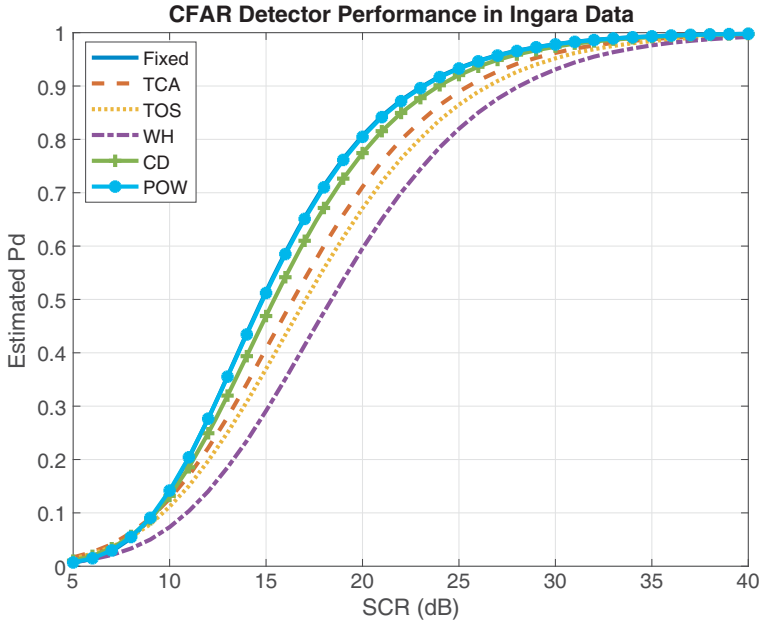

Figure 16. Detector performance in the Ingara data set run 34 683, at an azimuth angle of 225°, with horizontal transmit and receive polarisation.

Table 2. Resultant Pfa produced by the detectors running on the Ingara data. The absolute error is the norm of the difference of the estimated Pfa and the design Pfa, which is 10^{-4}.

Detector	Estimated Pfa	Absolute Error
TCA	1.7724×10^{-4}	7.7240×10^{-5}
TOS	1.8081×10^{-4}	8.8081×10^{-4}
WH	1.2252×10^{-4}	2.252×10^{-5}
CD	1.0944×10^{-4}	9.4400×10^{-6}
POW	8.8025×10^{-5}	1.1975×10^{-5}

6. CONCLUSIONS AND FURTHER RESEARCH

This paper examined the Burr distributional fit to DST Group's Ingara radar clutter and showed that it can provide improved fits relative to a Pareto Type II model. Based upon this, an examination of non-coherent detection processes was initiated. A series of five decision rules were derived and shown to possess varying degrees of the CFAR property. Some of these detectors were excellent at managing interference and clutter power transitions. Their performance in real data showed promising results.

This analysis has opened up the opportunity for further development and analysis. Firstly it would be of interest to validate the Burr distributional fit to other X-band high resolution maritime surveillance radar clutter sets. Secondly, it is of interest to investigate the existence of a non-coherent detection process which is CFAR with respect to the three distributional parameters.

In addition to this, it is of relevance to examine whether the Burr distributional model can be embedded within a compound Gaussian process with a specific texture distribution. This would provide further credibility for the application of the Burr distributional model to maritime surveillance radar clutter modelling. Furthermore, this would justify the development of coherent multilook detection processes with such an intensity model.

REFERENCES

1. Minkler, G. and J. Minkler, *CFAR: The Principles of Automatic Radar Detection in Clutter*, Magellan, Baltimore, 1990.
2. Weinberg, G. V., *Radar Detection Theory of Sliding Window Processes*, CRC Press, 2017, ISBN 9781498768184.
3. Balleri, A., A. Nehorai, and J. Wang, "Maximum likelihood estimation for compound-gaussian clutter with inverse-Gamma texture," *IEEE Transactions on Aerospace and Electronic Systems*, Vol. 43, 775–779, 2007.
4. Farshchian, M. and F. L. Posner, "The Pareto distribution for low grazing angle and high resolution X-band sea clutter," *IEEE Radar Conference Proceedings*, 789–793, 2010.
5. Weinberg, G. V., "Assessing Pareto fit to high resolution high grazing angle sea clutter," *IET Electronics Letters*, Vol. 47, 516–517, 2011.
6. Burr, I. W., "Cumulative frequency functions," *Annals of Mathematical Statistics*, Vol. 13, 215–232, 1942.
7. Stacy, N. J. S., M. P. Burgess, M. R. Muller, and R. Smith, "Ingara: An integrated airborne imaging radar system," *Proceedings of the International Geoscience and Remote Sensing Symposium*, 1618–1620, 1996.
8. Stacy, N., D. Crisp, A. Goh, D. Badger, and M. Preiss, "Polarimetric analysis of fine resolution X-band sea clutter data," *Proceedings of the International Geoscience and Remote Sensing Symposium*, 2787–2790, 2005.
9. Crisp, D. J., N. J. S. Stacy, D. A. Hudson, P. B. Pincus, and A. S. Goh, "Polarimetric analysis of maritime SAR data collected with the DSTO ingara X-band radar," *Proceedings of the International Geoscience and Remote Sensing Symposium*, 3870–3873, 2007.
10. Crisp, D. J., L. Rosenberg, N. J. Stacy, and Y. Dong, "Modelling X-band sea clutter with the K-distribution: Shape parameter variation," *Proceedings of the International Radar Conference-Surveillance for a Safer World*, 1–6, 2009.
11. Weinberg, G. V., "Constant false alarm rate detectors for Pareto clutter models," *IET Radar, Sonar and Navigation*, Vol. 7, 153–163, 2013.
12. Weinberg, G. V., "General transformation approach for constant false alarm rate detector development," *Digital Signal Processing*, Vol. 30, 15–26, 2014.
13. Weinberg, G. V., "Management of interference in Pareto CFAR processes using adaptive test cell analysis," *Signal Processing*, Vol. 104, 264–273, 2014.
14. Weinberg, G. V., "Development of an improved minimum order statistic detection process for Pareto distributed clutter," *IET Radar, Sonar and Navigation*, Vol. 9, 19–30, 2015.
15. Weinberg, G. V., "Examination of classical detection schemes for targets in Pareto distributed clutter: Do classical CFAR detectors exist, as in the Gaussian case?," *Multidimensional Systems and Signal Processing*, Vol. 26, 599–617, 2015.
16. Weinberg, G. V., "On the construction of CFAR decision rules via transformations," *IEEE Transactions on Geoscience and Remote Sensing*, Vol. 55, 1140–1146, 2017.
17. Finn, H. M. and R. S. Johnson, "Adaptive detection model with threshold control as a function of spatially sampled clutter-level estimates," *RCA Review*, Vol. 29, 414–464, 1968.

18. Gandhi, P. P. and S. A. Kassam, "Analysis of CFAR processors in nonhomogeneous background," *IEEE Transactions on Aerospace and Electronic Systems*, Vol. 24, 427–445, 1988.
19. Weinberg, G. V., "An invariant sliding window detection process," *IEEE Signal Processing Letters*, Vol. 24, 1093–1097, 2017.
20. Beaumont, G. P., *Intermediate Mathematical Statistics*, Chapman and Hall, London, 1980.
21. Ross, S. M., *Simulation*, 5th Edition, Academic Press, 2012.
22. Weinberg, G. V., "Estimation of Pareto clutter parameters using order statistics and linear regression," *IET Electronics Letters*, Vol. 49, 845–846, 2013.
23. Jakeman, E. and P. N. Pusey, "A model for non-Rayleigh sea echo," *IEEE Transactions on Antennas and Propagation*, Vol. 24, 806–814, 1976.
24. Ward, K. D., "Compound representation of high resolution sea clutter," *IEE Electronics Letters*, Vol. 17, 561–563, 1981.
25. Watts, S., "Radar detection prediction in sea clutter using the compound K-distribution model," *IEE Proceedings F*, Vol. 132, 613–620, 1985.
26. Weibull, W., "A statistical distribution function of wide applicability," *ASME Journal of Applied Mechanics*, Vol. 18, 293–297, 1951.
27. Sekine, M. and Y. Mao, *Weibull Radar Clutter*, IET, UK, 1990.
28. Tao, D., S. N. Anfinsen, and C. Brekke, "Robust CFAR detector based on truncated statistics in multiple-target situations," *IEEE Transactions on Geoscience and Remote Sensing*, Vol. 54, 117–134, 2016.
29. Tao, D., A. P. Doulgeris, and C. Brekke, "A segmentation-based CFAR detection algorithm using truncated statistics," *IEEE Transactions on Geoscience and Remote Sensing*, Vol. 54, 2887–2898, 2016.
30. Dai, H., L. Du, Y. Wang, and Z. Wang, "A modified CFAR algorithm based on object proposals for ship target detection in SAR images," *IEEE Geoscience and Remote Sensing Letters*, Vol. 13, 1925–1929, 2016.
31. Gao, G. and G. Shi, "CFAR ship detection in nonhomogeneous sea clutter using polarimetric SAR data based on the notch filter," *IEEE Transactions on Geoscience and Remote Sensing*, Vol. 55, 4811–4824, 2017.
32. Izzo, A., M. Liguori, C. Clemente, C. Galdi, M. Di Bisceglie, and J. J. Soraghan, "Multimodel CFAR detection in foliage penetrating SAR images," *IEEE Transactions on Aerospace and Electronic Systems*, Vol. 53, 1769–1780, 2017.
33. Wang, C., F. Bi, W. Zhang, and L. Chen, "An intensity-space domain CFAR method for ship detection in HR SAR images," *IEEE Geoscience and Remote Sensing Letters*, Vol. 14, 529–533, 2017.
34. Ai, J., X. Yang, J. Song, Z. Dong, L. Jia, and F. Zhou, "An adaptively truncated clutter-statistics-based two-parameter CFAR detector in SAR imagery," *IEEE Journal of Oceanic Engineering*, Vol. 43, 267–279, 2018.
35. Lu, S., W. Yi, W. Liu, G. Cui, L. Kong, and X. Yang, "Data-dependent clustering-CFAR detector in heterogeneous environment," *IEEE Transactions on Aerospace and Electronic Systems*, Vol. 54, 476–485, 2018.
36. Li, T., Z. Liu, R. Xie, and L. Ren, "An improved superpixel-level CFAR detection method for ship targets in high-resolution SAR images," *IEEE Journal of Selected Topics in Applied Earth Observations and Remote Sensing*, Vol. 11, 184–194, 2018.
37. Zhao, W., J. Li, X. Yang, Q. Peng, and J. Wang, "Innovative CFAR detector with effective parameter estimation method for generalised Gamma distribution and iterative sliding window strategy," *IET Image Processing*, Vol. 12, 60–69, 2018.
38. Weinberg, G. V., L. Bateman, and P. Hayden, "Constant false alarm rate detection in Pareto Type II clutter," *Digital Signal Processing*, Vol. 68, 192–198, 2017.